

Wavelength-dispersive double flat-crystal analyzer for inelastic X-ray scattering

G. Bortel,*† E. E. Alp, W. Sturhahn and T. S. Toellner

Advanced Photon Source, Argonne National Laboratory, Argonne IL 60439, USA.

E-mail: gb@szfki.hu

(Received 5 November 1999; accepted 3 July 2000)

A double flat-crystal analyzer for inelastic X-ray scattering is described. The general correlation between the energy and direction of the X-rays transmitted by the analyzer allows one to collect data for a range of energy transfers simultaneously. Such an analyzer with 120 meV resolution was built to operate at the copper *K* edge. Experimental results show that this X-ray optic can be an alternative to a conventional spherical-focusing backscattering analyzer in resonant inelastic X-ray scattering experiments or when flexible energy resolution or high momentum resolution is required.

Keywords: X-ray optics; crystal analyzers; resonant/anomalous inelastic X-ray scattering; absorption edges; electronic and vibrational excitations; parallel data collection.

1. Introduction

Inelastic X-ray scattering is used for the investigation of electronic structure and excitations of materials (Schülke, 1991). The atomic vibrations in solids or liquids can also be studied with high-energy-resolution instruments (Burkel, 1991). In an inelastic X-ray scattering experiment the energy and momentum transfer to the sample has to be measured. In resonant experiments the absolute value of the photon energy is equally important (Platzman & Isaacs, 1998). Measurements performed on single crystals also require orientation of the scattering vector along specific lattice directions. Experimental control of these values is most commonly achieved in an instrument consisting of a monochromator-analyzer pair and a goniometer for the sample.

The backscattering geometry, *i.e.* a Bragg reflection with Bragg angle close to 90° (Graeff & Materlik, 1982), has been used to build analyzers in the sub-eV energy-resolution range. Such reflections possess weak energy dispersion, increased angular acceptance and good energy resolution compared with a non-backscattering reflection. Spherical-focusing backscattering analyzers (Dorner *et al.*, 1986) present the common solution for most of the inelastic X-ray scattering experiments. Unfortunately, these analyzers cannot be prepared for arbitrary X-ray energies but only for those that are close to meeting the backscattering condition. In resonant inelastic X-ray scattering experiments, where the photon energy has to be in the vicinity of a given absorption edge, the performance of a single-reflection analyzer is usually poor. To overcome this limitation in general, one has to seek another X-ray optic.

We suggest the use of a double flat-crystal arrangement, which has been discussed elsewhere (Beaumont & Hart, 1974; Nakayama *et al.*, 1973) and was recently used for high-resolution monochromatization (Ishikawa *et al.*, 1992; Toellner, 1996, 2000; Chumakov *et al.*, 1996; Toellner *et al.*, 1997). These monochromators consist of two perfect crystals and the usually high-index Bragg reflections are in dispersive arrangement. The crystals are strongly asymmetrically cut in the opposite sense such that the first reflection has increased angular acceptance. The bandwidth of these monochromators is typically in the meV range.

The above-mentioned limitations of the spherical-focusing backscattering analyzers (SFBA) and the development of high-resolution monochromators suggest employment of a double flat-crystal monochromator as an analyzer for inelastic X-ray scattering. The double flat-crystal analyzer (DFCA) has been touched upon briefly in the literature (Schülke, 1991) but has never received further attention. In this paper we discuss the expected behavior of a DFCA, show the results of the first test experiment we carried out and make a comparison with an SFBA. We would like to emphasize at this point that the same X-ray optic used as a monochromator or analyzer can behave quite differently owing to the nature of the incident radiation. If the X-ray beam to be monochromated originates from an undulator source, it will be well collimated with divergences of a few times 10 μ rad. However, the radiation emerging from a sample after an inelastic-scattering process is much more divergent. The influence of this divergence on the transmission properties of a double flat-crystal X-ray optic is the subject of this paper. We will show that this altered condition leads to an energy dispersion that can be advantageously exploited in analyzer applications for inelastic-scattering experiments.

† On leave from Research Institute for Solid State Physics and Optics, H-1525 Budapest, POB 49, Hungary.

2. Description of the optic

Transmission properties in the energy–angle–position space of the DFCA, *i.e.* two successive Bragg reflections in dispersive arrangement, can be described using Bragg's law and simple geometry (Fig. 1). If an X-ray beam is reflected by both crystals in one common xy (vertical) scattering plane, the normal to the atomic planes can be written in the form

$$\mathbf{s}_1 = (\sin \theta_1, \cos \theta_1, 0), \quad \mathbf{s}_2 = (-\sin \theta_2, \cos \theta_2, 0). \quad (1)$$

The Bragg condition for these reflections with d_1 and d_2 lattice spacings at energy E_0 requires that

$$\sin \theta_1 = hc/(2d_1 E_0), \quad \sin \theta_2 = hc/(2d_2 E_0). \quad (2)$$

In our choice of coordinate system, the wavevector of the radiation between the crystals is parallel to the x axis. With the crystals in this optimized position for transmitting the ray with energy E_0 in the central scattering plane, we can investigate the possibility for a beam to be reflected by both crystals with another energy in any other direction. If a unit vector \mathbf{e}_{12} indicates the propagation direction of this ray with energy E between the two crystals, then the reflection conditions are the following,

$$\mathbf{e}_{12} \mathbf{s}_1 = hc/(2d_1 E), \quad -\mathbf{e}_{12} \mathbf{s}_2 = hc/(2d_2 E). \quad (3)$$

Solving these equations for \mathbf{e}_{12} we arrive at

$$\mathbf{e}_{12} = [E_0/E, 0, \pm(1 - E_0^2/E^2)^{1/2}]. \quad (4)$$

Introducing γ , the out-of-central scattering plane angle of this vector with $(\mathbf{e}_{12})_z = \sin \gamma$, we can write

$$\gamma = \pm \arccos(E_0/E) \quad \text{or} \quad E = E_0/\cos \gamma. \quad (5)$$

This simple result shows some interesting features. First of all the energy–angle correlation does not contain d_1 nor d_2 ; it is independent of the material and the reflections we have chosen. It is related to the principal energy E_0 only. The

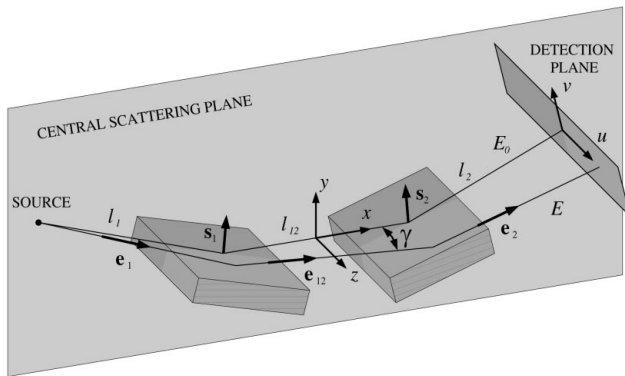


Figure 1

Schematic design of the DFCA showing the source of divergent radiation, the two asymmetrically cut crystals and the area detector. The central scattering plane is defined by the source and the common scattering plane of the beam with energy E_0 . The unit vectors \mathbf{s} and \mathbf{e} indicate the normal of the atomic planes and the propagation direction of the X-rays, respectively. l_1 , l_{12} and l_2 measure the distance between the source and detector along the path of the X-rays with E_0 energy in the central plane.

optic does not transmit X-rays below this energy, but it is able to reflect higher energies with a corresponding increase of the γ angle. This property is important for analyzer applications. The energy resolution, for example, is strongly affected if photons are collected in a large solid angle without directional discrimination.

Next we relate the horizontal displacement of the X-rays to their energy. From simple vector calculations the \mathbf{e}_1 incoming and \mathbf{e}_2 outgoing direction of the reflected X-rays (see Fig. 1) are

$$\mathbf{e}_1 = \mathbf{e}_{12} - 2(\mathbf{e}_{12} \mathbf{s}_1) \mathbf{s}_1, \quad \mathbf{e}_2 = \mathbf{e}_{12} - 2(\mathbf{e}_{12} \mathbf{s}_2) \mathbf{s}_2. \quad (6)$$

One can see that the e_z component and the γ angle are conserved through the Bragg reflections, since \mathbf{s} vectors have zero z components. This means that the energy–angle correlation for the radiation before the first and after the second reflection is still valid. Therefore, placing our plane of detection at pathlength $l = l_1 + l_{12} + l_2$ from the source, the out-of-plane (horizontal) deviation u of a beam passing through the analyzer is related to its energy according to

$$u = l \tan \gamma = \pm l (E^2/E_0^2 - 1)^{1/2}. \quad (7)$$

This energy–position correlation (Fig. 2a) gives the possibility of building an energy-dispersive instrument enabling one to determine the energy from the position by using the inverse formula

$$E = E_0(u^2/l^2 + 1)^{1/2}. \quad (8)$$

For a real experiment, however, the above expressions are not fully descriptive, since l is not a constant but shows a distribution, because of both the finite illuminated sample (hereafter source) size and the asymmetry of the Bragg reflections. The effect of these geometrical factors can be taken into account with the help of a ray-tracing simulation, assuming an extended source and an image plane. Based on the correlation between the \mathbf{e}_1 , \mathbf{e}_{12} , \mathbf{e}_2 directions and energy E , one can construct the image of the source for any energy (Fig. 2b). The calculation includes all geometrical parameters of the actual optic, the Bragg and asymmetry angles, the distances and the source size. The image of the source becomes distorted as we move away from the principal energy. Also, the resolving power in energy derived from the position is limited by the possible overlap between the spots belonging to different energies, especially far above E_0 . The overlap depends on the source size, the source-to-detector distance and the energy range above E_0 we want to cover with the analyzer.

We have already given an adequate description of the energy–angle–position correlation obtained from Bragg's law assuming zero reflection width and unit reflectivity. However, to provide a more realistic simulation of the transmission of the optic one has to include dynamical properties of the reflections, such as width and reflectivity, and also assume a divergent extended source with a non-zero energy bandwidth. The intensity in one point of the detection plane is a combination of partial transmissions of X-rays from all source points with all energies present in

the source. We carried out such a calculation, and the result (Fig. 2c) is a more realistic smeared intensity distribution. The simulation is in excellent agreement with the measured intensity distribution (Fig. 2d) explained in more detail in the following section.

To demonstrate the feasibility of the above-described optic, we built a DFCA working at 8979 eV, the copper *K* edge, with about 120 meV energy resolution. Optimization of the analyzer required the appropriate choice of reflections and asymmetry factors to meet the best possible combination of acceptance, throughput and resolution. The calculation of these quantities can be performed in a manner similar to the case of perfect crystal monochromators (Matsushita & Hashizume, 1983). The following guidelines were considered: (i) the energy resolution can be improved by choosing either higher index reflections or higher asymmetry angles; (ii) choosing higher index reflections decreases the angular acceptance, while increasing asymmetry reduces the reflectivity but improves the angular acceptance of the analyzer; (iii) the acceptance of the second reflection should match the emittance of the first reflection, otherwise a portion of the radiation is lost;

(iv) the intensity loss in the Bragg reflection at high asymmetry angles due to specular reflection from the surface sets a practical limit on the asymmetry of the crystals. Since we were interested in the largest angular acceptance with a moderate energy resolution, we chose the lowest index reflection with the highest asymmetry. Both of our reflections were Si(111) with asymmetry angles of $\pm 12.3^\circ$. The Bragg angle is 12.7° , while the critical angle is 0.2° at this energy. The asymmetry factors are 60 and 1/60, the calculated acceptance of the analyzer in the central scattering plane is 243 μrad and the energy resolution is 85 meV for a collimated beam and 117 meV for vertically divergent radiation.

3. Experiment

The experiment was performed at sector 3-ID of the Advanced Photon Source. The experimental setup is shown in Fig. 3. In order to map out the transmission properties of the DFCA, we needed a source of divergent monochromatic radiation with bandwidth smaller than or comparable with the intrinsic energy resolution of the analyzer. We

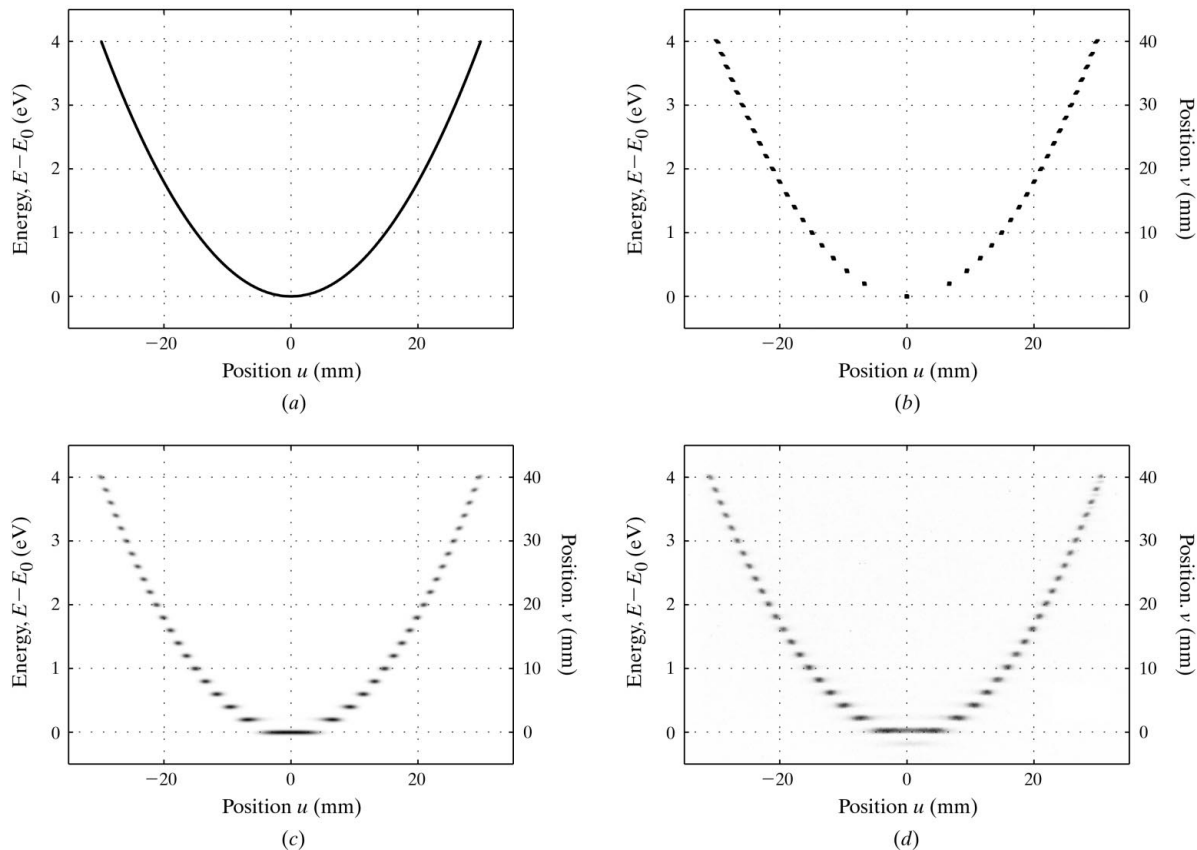


Figure 2

Representations of the energy–position correlation of the X-rays transmitted by the DFCA. (a) The analytical relationship expressed by equation (8). The solid line corresponds to the case of a monoenergetic point source treated within the kinematic theory. (b) Simulated intensity distribution in the plane of detection for an extended source for several discrete energy values above the principal energy. (c) Same as before, but the bandwidth of the source and dynamical properties of the reflections, *i.e.* reflectivity and width, are also taken into account. (d) The measured intensity distribution on the image plate. In (b), (c) and (d), note the artificial 2 mm v vertical translation at each 200 meV step of the energy of the monochromator. For each case, principal energy: 8979 eV; reflections: Si(111); asymmetry factors: 60 and 1/60; source-to-detector distance: 200 + 200 + 600 mm; source size: 0.5 mm \times 0.5 mm; source bandwidth: 65 meV.

used an Si(444) channel-cut crystal for monochromatization and an amorphous scatterer to produce the divergent radiation.

The measured bandwidth of the direct beam was 65 meV, and the flux in a beam of size $0.5 \text{ mm} \times 0.5 \text{ mm}$ was $5 \times 10^{10} \text{ photons s}^{-1}$. The energy was calibrated using the absorption edge of a copper foil. The prealignment of the two analyzer crystals, including the Bragg and tilt angles and positions, was performed in the collimated direct beam without scatterer. The combined energy resolution of the monochromator and analyzer was 110 meV, which implies that the intrinsic energy resolution of the analyzer is 89 meV, close to the expected value. This setup also gave us the opportunity to measure the vertical acceptance of the analyzer, which was $210 \mu\text{rad}$. The small deviation from the calculated values can be explained by a small discrepancy in the asymmetry angles. The 30% ratio of the intensities measured before and after the analyzer agrees well with the calculated 48% value if we take into account the 68% transmission of the additional air in the beam path.

Next we investigated the analyzer in the divergent radiation. The analyzer was turned to a 15° scattering angle corresponding to the maximum intensity of the Debye-Scherrer ring of the plexiglass scatterer. For detection of radiation transmitted by the analyzer, we used a scintillation counter with an adjustable aperture mounted on a double translation stage at 1 m pathlength from the scatterer. This allowed us to move the detector to any position in the plane of detection. Alternatively, we also used an image plate as an area detector. It was mounted on a vertical translation stage, permitting us to record multiple images in the same exposure.

A way to verify the energy–position correlation experimentally is to record images of the intensity distribution behind the analyzer for several monochromator energies (E), keeping the analyzer crystals fixed, transmitting the principal energy (E_0) in the central scattering plane. If we translate the image plate in the vertical direction each time we change E , we can directly plot the above-derived relationship (Fig. 2*d*). Note that we applied this translation in

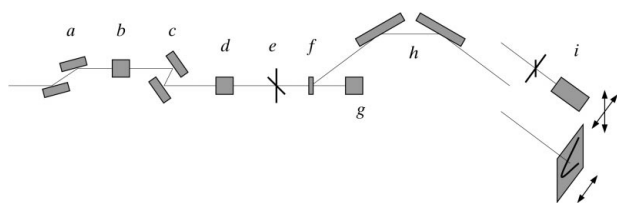


Figure 3

Experimental setup at the 3-ID beamline of the Advanced Photon Source for characterizing the X-ray transmission properties of the DFCA. (a) Diamond premonochromator. $E = 8979 \text{ eV}$, $\Delta E \simeq 600 \text{ meV}$. (b) Ionization chamber. $\Phi \simeq 10^{13} \text{ photons s}^{-1}$. (c) Si(444) monochromator. $\Delta E = 65 \text{ meV}$. (d) Ionization chamber. $\Phi \simeq 3 \times 10^{11} \text{ photons s}^{-1}$. (e) Slit, typically $0.5 \text{ mm} \times 0.5 \text{ mm}$. (f) Amorphous scatterer, plexiglass. (g) Pin diode, monitor. $\Phi \simeq 10^{10} \text{ photons s}^{-1}$. (h) Si(111) double flat-crystal analyzer, $\Delta E = 120 \text{ meV}$. (i) Detectors on translation stages: scintillation counter with slit or image plate. $\Phi \simeq 100 \text{ photons s}^{-1}$.

the measurement and in the calculations as well just to clearly separate the response of the analyzer at different energies. In fact, the spots lie on a horizontal line, and one needs a linear detector with a vertical acceptance of only a few mm. As we can see in Fig. 2(*d*), the two branches were limited to 4 eV above the principal energy. This limitation resulted from the 25 mm width of the analyzer crystals and their smallest possible distance to the source. Indeed, when we shifted the crystals sideways, we could observe one branch of the energy–position curve up to 12 eV above E_0 , still limited by the size of the crystals. The 200 mm length of the crystals together with the 0.4° grazing angle of the X-rays are also important factors. These determine the vertical spatial acceptance of the analyzer. In our case it was 1.4 mm, which is larger than the source size.

The intensity distribution on the image plate (Fig. 4*a*) can be converted into energy spectra (Fig. 4*c*). The image-plate readings were calibrated by comparing them with the counts from the scintillation detector. Then the images were integrated along the vertical direction resulting in one-dimensional intensity distributions (Fig. 4*b*). Using a linear detector, one would immediately measure these data as a function of the horizontal coordinate. The center of these data was determined based on their symmetry. Finally the energy scale was obtained using equation (8), knowing E_0 and l . Throughout this process we corrected the

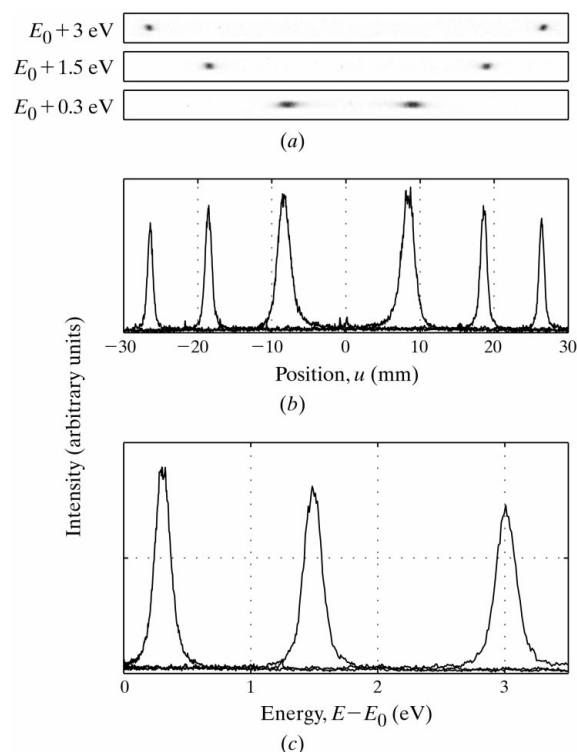


Figure 4

Illustration of position to energy conversion. The image-plate data (a) and the corresponding one-dimensional data (b) are shown for three monochromator energy settings above the principal energy. The energy scale in (c) was obtained from equation (8), using $E_0 = 8979 \text{ eV}$ and $l = 1000 \text{ mm}$.

measured intensities to compensate for the incoming intensity variations and for air absorption.

Beyond demonstrating the conversion of the positional information to energy spectra, we also derived two important figures characteristic to the transmission properties of this DFCA: the angle-integrated transmission and the energy resolution. Both depend on the deviation of the X-rays from the central scattering plane and therefore on the energy above E_0 . In the next two paragraphs we explain the derivation of these quantities.

We know that the bandwidth and size of the source are smaller than the energy resolution and spatial acceptance of the analyzer. Therefore the intensity loss caused by the analyzer resides mainly in its limited angular acceptance and in the reflectivity of the crystals. One can see that the flux (photons s^{-1}) after the analyzer normalized with the brightness (photons $mrad^{-2} s^{-1}$) before the analyzer gives the angle-integrated transmission of the optic (Fig. 5*a*). We can roughly think of this quantity as the solid angular

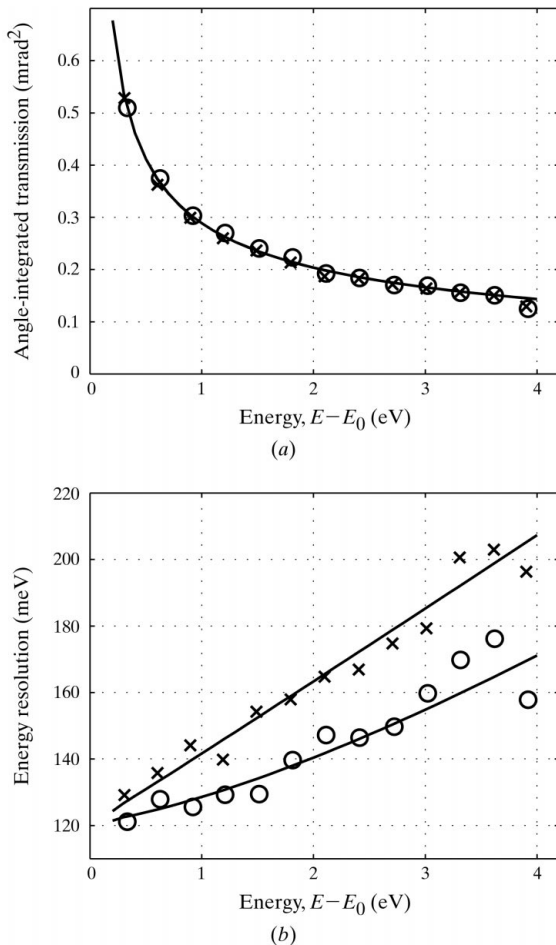


Figure 5 The measured angle-integrated transmission (*a*) and the energy resolution (*b*) of the DFCA. The \circ and \times symbols represent $0.25 \text{ mm} \times 0.25 \text{ mm}$ and $0.5 \text{ mm} \times 0.5 \text{ mm}$ source sizes, respectively. The solid lines are results from simulations and are explained in the text. While the angle-integrated transmission is independent of the source size, the energy resolution contains geometrical contributions.

acceptance. The brightness of the source, *i.e.* the amorphous scatterer, was measured independently using the same source and detector with a slit but no analyzer. The angle-integrated transmission shows a monotonic decrease with increasing energy.

Since we had an elastic scatterer as a source, the width of the peaks in the obtained energy spectra is the instrumental energy resolution including both the monochromator and the DFCA. The resolution of the analyzer can be obtained from the total width of the instrumental resolution function by deconvolving the previously determined 65 meV bandwidth of the probing radiation (Fig. 5*b*). The typical error of the energy resolution determined this way is $\pm 5 \text{ meV}$. We can see that the bandwidth is best at E_0 . The monotonic increase with increasing energy originates from geometrical effects, related mainly to the source size, as is shown by the two sets of points.

In inelastic scattering experiments an important parameter of the applied optic is suppression of the elastic signal when measuring the inelastic part of the energy spectrum. We have attempted to determine this for the DFCA by recording the intensity at several points that do not lie on the energy–position dispersion curve of the elastic peak. However, our measurement also includes other sources, such as the electronic noise of the detection system ($0.01 \text{ photons s}^{-1}$), background radiation from air scattering, and possibly some inelastic scattering from our plexiglass sample. The measured counts at 10, 2 and 1 eV from the elastic peak were 0.04, 0.05 and 0.14 photons s^{-1} , respectively, while the elastic intensity was 40 photons s^{-1} . Assuming that the counts at 10 eV come equally from the above sources, we can estimate a suppression of a few thousand at 2 eV and a few hundred at 1 eV from the elastic peak. This good performance is primarily related to the use of two reflections.

As an example, we measured inelastic scattering from polycrystalline beryllium (Fig. 6). The scattering angle was set to correspond to a momentum transfer of 1.18 \AA^{-1} . This

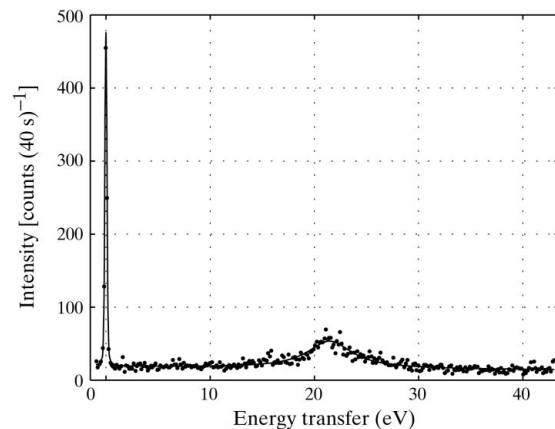


Figure 6 The raw data of inelastic X-ray scattering from polycrystalline beryllium. The broad peak at an energy transfer of 21.5 eV results from plasmon excitations. The momentum transfer was 1.18 \AA^{-1} . The solid line is a fitted curve.

is approximately 90% of the plasmon cutoff wavevector in beryllium. The 5 eV broad inelastic peak centered at an energy transfer of 21.5 eV is in agreement with the value in the literature (Schülke *et al.*, 1989). Although the spectrum was collected by scanning the energy using a single-element detector in the central scattering plane, it clearly demonstrates the good energy resolution and large accessible energy range of the analyzer.

4. Discussion

Fig. 5 shows the angular acceptance and energy resolution of the analyzer. The corresponding calculated curves obtained from the simulation of the transmission properties of the optic (Fig. 2c) are represented by solid lines. The good agreement indicates that all important factors have been taken into account. Both plots show that the analyzer works most efficiently in the central plane at energy E_0 . Geometrical factors start to weaken the performance with deviation from E_0 . Nevertheless, in an inelastic scattering experiment where the measurement is taken with positive energy transfer to the sample, the inelastic part is measured more efficiently than the elastic peak. Let us consider a resonant experiment in which we have to keep the monochromator energy at the threshold energy E_r . If we expect an inelastic feature at energy transfer E_i , we should tune the principal energy of the analyzer to or slightly below $E_r - E_i$. In this case the energy transfer E_i to the sample is observed in or close to the central scattering plane with optimal angular acceptance and energy resolution. The elastic peak appears further away. If the energy range of the analyzer is not sufficient to cover both the elastic peak and the inelastic features, one can still place the energy window on the interested range of the spectrum and take advantage of parallel data collection. Clearly, the DFCA should be used along with a position-sensitive detector (PSD) to fully exploit its transmission properties. The gain compared with a single detector mode can be 10–50 depending mainly on the energy range covered by the analyzer.

Beyond the energy-dispersive property of the DFCA, another noteworthy feature is the extremely good momentum resolution, which is important when a measurement is performed close to the direct beam or a Bragg peak or in cases of small Brillouin zones or strong energy–momentum dispersion. If, for example, we consider a crystal with lattice parameter 10 Å and we require a momentum resolution better than one-tenth of the size of the Brillouin zone, we arrive at a momentum resolution requirement of 0.06 \AA^{-1} . The momentum resolution of a DFCA can be determined from geometrical factors and from the angular acceptance of the first reflection. In our case of source size 0.5 mm, pathlength 1 m and vertical acceptance $200 \mu\text{rad}$, the definition of the solid angle is $500 \mu\text{rad} \times 200 \mu\text{rad}$. This solid angle corresponds to a momentum resolution better than 0.003 \AA^{-1} over the whole range of scattering angles. Although an energy

spectrum collected simultaneously by the analyzer is just approximately a constant momentum-transfer scan, all the points in the spectrum represent a well defined scattering vector and the energy–momentum transfer space is mappable with this resolution. The good momentum resolution of the DFCA also makes possible inelastic small-angle scattering experiments or scattering in grazing angle from thin films and layer structures.

In the following we give a numerical comparison between the DFCA presented in this paper and a Ge(733) SFBA providing similar performance (Abbamonte, 1999). The SFBA in question has 35 meV intrinsic energy resolution, and with optimized geometrical contributions the energy resolution is about 200 meV. At 8979 eV the Bragg angle is 2.7° away from exact backscattering, and the vertical angular acceptance is about $100 \mu\text{rad}$. The solid angle covered by the 76 mm-diameter 1 m-bending-radius analyzer is 5000 mrad^2 . Nevertheless, the real angular acceptance is about one-fifth of this, since the 0.5 mm pixel size results in a relative angle between adjacent pixels that is five times larger than the intrinsic reflection width. The horizontal acceptance is much larger; therefore the corresponding factor in that direction does not decrease the solid angle. Furthermore, to achieve the 0.06 \AA^{-1} momentum resolution expressed in the previous paragraph, one has to reduce the solid angle using an aperture. The actual shape of the aperture depends on the scattering angle, but its size is about 7 mrad in the scattering plane, reducing the solid angle by another factor of ten. This way the effectively accepted solid angle is about 100 mrad^2 . On the other hand, the described DFCA of resolution 120–200 meV has a vertical acceptance of about $200 \mu\text{rad}$, while the perpendicular acceptance is related to the energy range we cover with the analyzer. If we choose a typical 10 eV range corresponding to a $2 \times 50 \text{ mrad}$ horizontal angular range, then the total solid angular acceptance is 20 mrad^2 . Although the SFBA is used in energy-scanning mode while the DFCA is optimally used in a parallel data-collection mode, the integrated intensity in an energy spectrum collected in the same time period is proportional to the total solid angular acceptance in both cases. This way our simple estimate shows that the SFBA is about five times more efficient than the DFCA. There is a factor, however, which we could not include: the sensitivity of the SFBA to the perfection of the focusing geometry. This would presumably change the ratio in favor of the DFCA. Even with this ratio, however, the DFCA can be useful in some experiments if we consider its other advantages.

The principal energy and energy resolution of the DFCA are independent design parameters whereas, in the case of an SFBA, the resolution is mostly determined by the principal energy. For instance, one can build a DFCA for the same edge energy with a resolution of a few meV to a few hundred meV. The limit on the energy resolution at a given energy is set by the combination of the highest index reflection and the highest practical asymmetry angle. Therefore we were able to design and build a DFCA for the

same 8979 eV energy with 3.7 meV resolution using two Si(553) reflections with asymmetry factors of 30 and 1/30. This resolution should allow investigation of low-energy excitations from atomic vibrations in the vicinity of the absorption edge with the idea of obtaining element-specific information on the vibrational modes, dispersion and density of states. However, the narrow bandpass and decreased angular acceptance of this optic result in low integrated transmissions. In combination with present X-ray sources, the achievable counting rates are impractically low.

Finally, we summarize briefly the steps of designing a DFCA. The process should always start from the desired principal energy and energy resolution. The choice of the reflections and asymmetry angles then determines the reflectivity and the vertical acceptance. The energy range one wishes to cover with the analyzer defines the total horizontal acceptance. The geometrical factors, such as sample-to-detector distance, sample size, crystal size, length and resolution of the PSD, are also important design parameters. In view of these parameters, the feasibility of a planned experiment using a DFCA can be judged if the scattering strength of the sample is known.

5. Conclusions

We have investigated a novel analyzer optic suitable for inelastic X-ray experiments. The transmission properties of the optic were simulated and compared with measurements. The energy–angle–position correlation of the X-rays transmitted by the analyzer was described and the possibility of parallel data collection of energy spectra emerged. Advantages of the DFCA in certain experiments over the commonly used SFBA were identified, such as flexible principal energy and energy resolution, very good momentum resolution and good suppression ratio. Many of these features are related to the use of two perfect flat-crystal Bragg reflections. The feasibility of inelastic X-ray scattering experiments using DFCA was demonstrated in the case of beryllium plasmon excitations. This kind of analyzer used with a PSD can find its way to resonant inelastic scattering applications in the sub-eV and perhaps

in the meV resolution range. The exceptional momentum resolution can also lead to small or grazing-angle inelastic scattering experiments.

The authors would like to thank P. Lee, M. Hu and H. Sinn of Argonne National Laboratory for many useful discussions and for their help in the experiments. Use of the Advanced Photon Source was supported by the US Department of Energy, Basic Energy Sciences, Office of Energy Research, under Contract No. W-31-109-ENG-38.

References

- Abbamonte, P. M. (1999). PhD thesis, University of Illinois at Urbana-Champaign, Illinois, USA.
- Beaumont, J. A. & Hart, M. (1974). *J. Phys. E*, **7**, 823.
- Burkel, E. (1991). *Inelastic Scattering of X-rays with Very High Energy Resolution, Springer Tracts in Modern Physics*, Vol. 125, edited by G. Höhler & E. A. Niekisch. Berlin: Springer-Verlag.
- Chumakov, A. I., Metge, J., Baron, A. Q. R., Grünsteudel, H., Grünsteudel, H. F., Ruffer, R. & Ishikawa, T. (1996). *Nucl. Instrum. Methods A*, **383**, 642–644.
- Dorner, B., Burkel, E. & Peisl, J. (1986). *Nucl. Instrum. Methods A*, **246**, 450–451.
- Graeff, W. & Materlik, G. (1982). *Nucl. Instrum. Methods*, **195**, 97–103.
- Ishikawa, T., Yoda, Y., Izumi, K., Suzuki, C. K., Zhang, X. W., Ando, M. & Kikuta, S. (1992). *Rev. Sci. Instrum.* **63**, 1015–1018.
- Matsushita, T. & Hashizume, H. (1983). *Handbook on Synchrotron Radiation*, Vol. 1, edited by E. E. Koch, pp. 261–314. Amsterdam: North-Holland.
- Nakayama, K., Hashizume, H., Miyoshi, A., Kikuta, S. & Kohra, K. (1973). *Z. Naturforsch. Teil A*, **28**, 632.
- Platzman, P. M. & Isaacs, E. D. (1998). *Phys. Rev. B*, **57**, 11107–11114.
- Schülke, W. (1991). *Handbook on Synchrotron Radiation*, Vol. 3, edited by G. S. Brown & D. E. Moncton, pp. 565–637. Amsterdam: North-Holland.
- Schülke, W., Nagasawa, H., Mourikis, S. & Kaprolat, A. (1989). *Phys. Rev. B*, **40**, 12215–12228.
- Toellner, T. S. (1996). PhD thesis, Northwestern University, Evanston, Illinois, USA.
- Toellner, T. S. (2000). *Nuclear Resonant Scattering of Synchrotron Radiation*, Vol. 125, edited by E. Gerdau & H. de Waard, pp. 3–28. The Netherlands: Baltzer Science.
- Toellner, T. S., Hu, M., Sturhahn, W., Quast, K. & Alp, E. E. (1997). *Appl. Phys. Lett.* **71**, 2112–2114.